HHS Public Access

Author manuscript

Curr Biol. Author manuscript; available in PMC 2017 December 05.

Published in final edited form as:

Curr Biol. 2016 December 05; 26(23): 3129–3142. doi:10.1016/j.cub.2016.09.052.

Retromer endosome exit domains serve multiple trafficking destinations and regulate local G protein activation by GPCRs

Katherine C. Varandas[1], **Roshanak Irannejad**[2], and **Mark von Zastrow**[1,2,3]

[1]Program in Cell Biology, University of California San Francisco, 16th Street, San Francisco, CA 94158, USA

[2]Department of Psychiatry, University of California San Francisco School of Medicine, 16th Street, San Francisco, CA 94158, USA

[3]Department of Cellular and Molecular Pharmacology, University of California San Francisco, 16th Street, San Francisco, CA 94158, USA

SUMMARY

Retromer mediates sequence-directed cargo exit from endosomes to support both endosome-to-Golgi (retrograde transport) and endosome-to-plasma membrane (recycling) itineraries. It is not known if these trafficking functions require cargos to exit endosomes separately via distinct transport intermediates, or if the same retromer-coated carriers can support both itineraries. We addressed this question by comparing human Wntless (Wls) and β-2 adrenergic receptor (β2AR), which require retromer physiologically for retrograde transport and recycling, respectively. We show here, by direct visualization in living cells, that both cargos transit primarily the same endosomes and exit via shared transport vesicles generated from a retromer-coated endosome domain. While both Wls and β2AR clearly localize to the same retromer-coated endosome domains, Wls is consistently enriched more strongly. This enrichment difference is determined by distinct motifs present in the cytoplasmic tail of each cargo, with Wls using tandem Φ-X-[L/M] motifs and β2AR using a PDZ motif. Exchanging these determinants reverses the enrichment phenotype of each cargo but does not change cargo itinerary, verifying the multifunctional nature of retromer and implying that additional sorting must occur downstream. Quantitative differences in the degree of cargo enrichment instead underlie a form of kinetic sorting that impacts the rate of cargo delivery via both itineraries and determines the ability of β2AR to activate its cognate G protein transducer locally from endosomes. We propose that mammalian retromer forms a multifunctional membrane coat that supports shared cargo exit for divergent trafficking itineraries and regulates signaling from endosomes.

Contact: mark.vonzastrow@ucsf.edu.

AUTHOR CONTRIBUTIONS

KCV and MvZ conceived of the project. KCV conducted experiments and analysis with assistance from RI and supervision from MvZ. KV and MvZ wrote the manuscript.

INTRODUCTION

Retromer was discovered in *S. cerevisiae* through its role in retrieving membrane cargos from endosomes to Golgi membranes, the retrograde transport route [1,2]. In *S. cerevisiae*, retromer is a stable heteropentamer composed of a VPS26/29/35 heterotrimer, which mediates cargo selection by binding to sorting determinants present in cargo proteins, and a VPS5/17 heterodimer that deforms the endosome membrane for vesicle budding [1,3,4].

Retromer is deeply conserved, and mutations or alterations in expression of retromer components in humans have been associated with a variety of pathologies [5–7]. In mammals and other higher eukaryotes, retromer has additional trafficking functions [8]. Particularly, mammalian retromer supports cargo-selective endosome-to-plasma membrane recycling, as well as delivery to the trans-Golgi network (TGN) [9,10]. This recycling route is important for the regulation of various PDZ motif-bearing membrane cargos, including a number of signaling receptors [10]. Additionally, interactions between the mammalian VPS26/29/35 heterotrimer and the heterodimer of VPS5/17 homologues, the sorting nexin-BAR proteins SNX1, 2, 5, and 6, are weaker in mammals than *S. cerevisiae* [11–13]. Hence, mammalian retromer is generally defined as the VPS26/29/35 trimer, which associates with additional accessory proteins that confer specialized properties [10,14–16]. For example, sorting nexin 27 (SNX27) is required for retromer-dependent recycling of the β-2 adrenergic receptor (β2AR) [10,17] and sorting nexin 3 (SNX3) is required for retromer-dependent retrograde transport of the Wnt ligand transport protein, Wntless (Wls) [14,15].

Retromer is thought to form a coated domain of the endosome limiting membrane where cargos are selected for packaging into membrane intermediates that bud from the limiting membrane and are subsequently delivered to downstream destinations [1,8]. From this perspective, a fundamental question arises: how is the expanded diversity of retromer function is achieved? One possibility is that the discrete retrograde transport and recycling functions of retromer are mediated by the formation of separate retromer-containing coat complexes and exit carriers. According to this hypothesis, functional diversity of retromer is solved by the formation of biochemically distinct coat structures, each containing a different complement of accessory proteins and specialized to package recycling or retrograde cargos into distinct transport intermediates. Alternatively, retromer may have the ability to generate a multifunctional coat structure that packages cargos destined for both itineraries into shared intermediates. According to this hypothesis, retromer provides a flexible endosome exit site for multiple cargos, and must work in coordination with additional sorting downstream.

These hypotheses are not mutually exclusive but, to our knowledge, neither has been directly tested. We did so here by comparing β2AR and Wls, widely expressed mammalian retromer cargos that require recycling or retrograde transport, respectively, for their normal physiological operations [10,18–22]. We asked if these retromer-dependent cargos can transit the same endosomes and, if so, if their distinct itineraries require them to exit endosomes via different retromer-coated membranes. We show directly that both cargos transit the same endosomes and exit via a shared retromer-associated region of the endosome membrane. Independently verifying this conclusion, we show that endosome exit is mediated by discrete retromer sorting determinants in β2AR and Wls, but that each

determinant can support both itineraries. Together, our findings support the hypothesis that mammalian retromer has the capacity to generate truly multifunctional exit structures on endosomes. We also show that retromer mediates kinetic sorting that controls the ability of β2ARs to locally activate the heterotrimeric G protein, Gs, from the endosome membrane.

RESULTS

An experimental system for comparing cargo exit from endosomes

We focused on β2AR and Wls as retromer-dependent cargos with physiological recycling and retrograde transport itineraries, respectively [10,18–22], which require distinct accessory proteins to exit from endosomes [14,15,17]. β2AR and Wls are widely expressed in mammalian tissues, and are co-expressed in various cell lines including HEK-293 and HeLa cells that are widely used models of β2AR signaling and trafficking [23–26].

β2AR was tagged in its N-terminal extracellular domain with a Flag epitope (Flag-β2AR; Figure 1A), shown previously not to disrupt receptor function or trafficking [27,28]. Wls was tagged in its largest extracellular loop. Wild type Wls accumulates in the ER after endocytosis and retrograde transport [18–22,29], and the downstream, retromer-independent step of TGN-to-ER retrieval can be specifically blocked by epitope fusion to the intracellular C-terminus [24]. We verified this (Figure S1) and included a C-terminal HA epitope to generate a model cargo for examination of upstream, retromer-dependent trafficking (HA-Wls, Figure 1A). Validating this, HA-Wls was detectable in the plasma membrane by fluorescence microscopy of non-permeabilized cells and in permeabilized cells was most highly concentrated in TGN membranes defined by colocalization with TGN46 (Figure 1B). Both Flag-β2AR and HA-Wls trafficking remained retromer-dependent because RNAi-mediated depletion of VPS35 caused pronounced down-regulation of both model cargos (Figure 1C).

We identified transfection conditions to achieve similar levels of both tagged proteins in the plasma membrane, determined by fluorescence flow cytometry (Figure S2A). Because HA-Wls accumulates in the TGN at steady state, total cellular HA-Wls expression had to be adjusted ~10-fold higher than β2AR (Figure S2B). This corresponds to overexpression of ~5-fold relative to endogenous Wls (Figure S2B). Flag-β2AR expressed under similar experimental conditions was shown previously to achieve 5–10 fold overexpression relative to endogenous β2AR [23,30].

We then asked if this these conditions allow Flag-β2AR and HA-Wls to traffic differentially in the same cells. We first compared the localization of each model cargo at steady state in fixed, permeabilized cells. As expected, Flag-β2AR localized to the plasma membrane in the absence of agonist, and to the plasma membrane and endosomes after application of the β2AR agonist isoproterenol (Figure 1D). HA-Wls localized in the plasma membrane and endosomes, but was most highly concentrated in TGN membranes devoid of detectable Flag-β2AR, and this was insensitive to isoproterenol (Figure 1D).

We then labeled each cargo in the plasma membrane of living cells and examined the effect of a 60 minute 'chase' incubation in the presence of isoproterenol to allow endocytosis of

both Flag-β2AR (requires isoproterenol) and HA-Wls (constitutive) [29]. Cargos localized similarly in the plasma membrane before the chase incubation, and each achieved a distinct, cargo-appropriate intracellular localization pattern after the 60 minute chase (Figure 1E). We further established that co-expression of HA-Wls did not affect recycling of Flag-β2AR (Figure S2C) and, conversely, that co-expression of Flag-β2AR did not affect delivery of internalized HA-Wls to the TGN (Figure S2D and S2E). Together, these results validate the present experimental model and indicate that Flag-β2AR and HA-Wls can achieve distinct, cargo-appropriate itineraries within 60 minutes after endocytosis in the same cells.

Flag-β2AR and HA-Wls transit the same endosomes and retromer endosome domains

Having devised an experimental system that recapitulates distinct retromer-dependent itineraries, we investigated whether Flag-β2AR and HA-Wls transit the same or different endosomes, and whether they exit via the same or different retromer-associated carriers. In cells fixed after 15 minutes of chase incubation, Flag-β2AR and HA-Wls localized to the same internal membrane compartments (Figure 2A). Differences in Flag-β2AR and HA-Wls distribution became apparent in living cells, as chemical fixation causes endosomes to collapse, and using HEK-293 cells that typically have slightly larger endosomes [31]. Again, Flag-β2AR and HA-Wls localized to the same compartments and most were also marked by VPS29-mCherry, defining them as retromer-associated endosomes (Figure 2B). Verifying that these heterogeneously labeled structures indeed represent the same endosomes, both model cargos moved coordinately with retromer through the cytoplasm in live image series (Movie S1).

VPS29-mCherry localized to a protrusion of the endosome membrane that we generically called a ‘retromer endosome domain’ (RED). In the vast majority of endosomes examined, Flag-β2AR and HA-Wls were detected in the same REDs (Figure 2C and 2D). This was observed throughout the 60 minute chase incubation because, when images were separated into 10 min bins according to chase time, both cargos were observed in the same REDs in the majority of endosomes examined in all bins. Together, these data indicate that both Flag-β2AR and HA-Wls, representing model recycling and retrograde cargos, respectively, traverse the same endosomes and associate with the same REDs throughout the chase interval during which they achieve cargo-appropriate itineraries.

Flag-β2AR and HA-Wls exit endosomes via the same REDs but differ in degree of enrichment

Flag-β2AR and HA-Wls differed in their relative degree of enrichment in REDs (Figures 3A and 3B). To evaluate this across multiple images and experiments, we defined a ‘RED enrichment index’ as the mean fluorescence signal measured per pixel in the RED divided by that in the adjacent endosome region (Figure 3C, inset). Overall, the mean RED enrichment index determined across the 60 minute chase period was 0.59 for Flag-β2AR and 2.60 for HA-Wls (Figure 3C). As endosomes and REDs approach the lateral resolution limit of traditional light microscopy, we used structured illumination microscopy (SIM) to achieve higher resolution [32]. SIM verified that Flag-β2AR and HA-Wls localize in the same REDs and that HA-Wls is more highly enriched in REDs than Flag-β2AR (Figure S3). Although SIM provides enhanced spatial resolution, we were unable to achieve sufficient temporal

resolution to observed dynamic endosome movements due to slower acquisition. Therefore, we continued to utilize spinning disc confocal microscopy for subsequent analysis.

Because most REDs contained both Flag-β2AR and HA-Wls, we next investigated whether REDs define sites of shared cargo exit from endosomes. Small membrane vesicles were seen to bud off from REDs that contained both Flag-β2AR and HA-Wls and moved away from the donor endosome in live cell time series (Figure 3D; Movie S2). Similar to cargo enrichment in REDs, HA-Wls was more strongly enriched than Flag-β2AR in these exit vesicles. This was evident by line scan analysis of individual endosomes (Figure 3E) and across multiple endosomes by fluorescence intensity ratio in the exiting vesicles relative to donor endosomes (Figure 3F). Together, these observations support the hypothesis that REDs represent a region of the endosome limiting membrane where both recycling and retrograde transport cargos are packaged for exit from endosomes via a shared population of vesicular carriers.

A discrete sorting determinant in the Wls cytoplasmic tail that mediates cargo enrichment in REDs and is required for downstream delivery

We next sought to understand the structural basis for differential enrichment of Flag-β2AR and HA-Wls in REDs. β2AR associates with retromer through a C-terminal PDZ motif (Figure S4A, sequence i) that binds to SNX27 [10,17,18,33]. We reasoned that Wls must utilize a different sorting determinant to engage retromer because it does not possess a consensus PDZ motif at its C-terminus (Figure S4A, sequence ii) and can efficiently exit endosomes with an epitope tag fused to its C-terminus, a manipulation that blocks PDZ motif-directed exit of β2AR from endosomes [10,17,18,33].

Truncation of the distal 35 residues from the HA-Wls cytoplasmic tail (HA-WlsΔ35; Figure S4A, sequence iii), strongly reduced enrichment in REDs relative to the parental HA-Wls construct (Figures 4A and 4B). We isolated two regions within this 35 residue region that were each sufficient to mediate increased cargo enrichment in REDs, albeit to a reduced degree when compared to parental HA-Wls containing both regions (Figure S4A, sequences iv and v; Figures S4B–D). Both regions contain a consensus Φ-X-[L/M] motif [34,35], and point mutating them (HA-Wls(LQL+YKL>AAA); Figure S4A, sequence vi) reduced cargo enrichment in REDs (Figure 4C). Wls' Φ-X-[L/M] motifs are conserved across vertebrates except zebrafish, in which the hydrophobic residue in the first motif is replaced by threonine (Figure 4D). *Drosophila* and *C. elegans* Wls both lack Φ-X-[L/M] motifs, but contain two sequences conforming to [S/T]-X-[L/M] placed similarly in the cytoplasmic tail (Figure 4D).

We next examined whether this determinant is also required for subsequent delivery of HA-Wls to the TGN. In contrast to HA-Wls that colocalized extensively with TGN46 after 60 minute chase (Figure 4E), internalized HA-WlsΔ35 did not (Figure 4F). Internalized HA-Wls(LQL+YKL>AAA) was also strongly impaired in delivery to the TGN (Figure 4G). These results, quantified across multiple cells and experiments by Pearson's correlation analysis (Figure 4H), indicate that the discrete sorting determinant identified in Wls is indeed necessary for accumulation of internalized HA-Wls in the TGN.

Cargo-specific retromer sorting determinants affect trafficking kinetics but not overall itinerary

To investigate how discrete sorting determinants in Wls and β2AR might differ, we examined the consequences of exchanging them between model cargos. The RED enrichment of internalized β2AR is the same whether tagged with a HA or Flag epitope (Figure 5A), allowing mutational effects on cargo enrichment in REDs to be compared directly to that of wild type β2AR in the same endosomes. When the cytoplasmic determinant identified in Wls was exchanged for the PDZ motif-containing determinant present in Flag-β2AR, choosing junction points to maintain similar lengths of exchanged sequence in an effort to position the exchanged determinant properly, the mutant receptor (Flag-β2ARΔ42-Wls35) enriched more strongly in the same REDs than co-expressed HA-β2AR (Figure 5B).

Remarkably, Flag-β2ARΔ42-Wls35 recycled to the plasma membrane with efficiency indistinguishable from that of Flag-β2AR, and this was indeed a consequence of adding Wls-derived sequence rather than removing cytoplasmic sequence from β2AR (Figure 5C). Further, Flag-β2ARΔ42-Wls35 did not accumulate in TGN membranes more than the parental Flag-β2AR (Figures S5A and S5B). Moreover, and fully consistent with its enhanced enrichment in REDs, the Wls-derived sorting determinant significantly increased the rate at which mutant β2ARs recycle to the plasma membrane (Figure 5D).

We then examined the effect of making the converse exchange, again choosing junction points to maintain similar lengths of exchanged sequence to position the exchanged determinant properly. Replacing the cytoplasmic sequence identified in Wls with that derived from β2AR (HA-WlsΔ35-β2AR42) strongly reduced enrichment in REDs, making it indistinguishable from that observed for co-expressed Flag-β2AR (Figures 5E and 5F). However, internalized HA-WlsΔ35-β2AR42 still strongly accumulated in the TGN after 60 minutes of chase incubation (Figure 5G, Figure S5C), and this depended on the β2AR-derived tail sequence added rather than Wls tail sequence removed (Figure 5G). Time-dependent Pearson's correlation coefficient analysis revealed that HA-WlsΔ35-β2AR42, despite localizing at long chase time in the TGN similarly to HA-Wls, accumulates there more slowly (Figure 5H). Together these data support the hypothesis that differences in cargo enrichment in REDs, as conferred by the discrete cytoplasmic sorting determinants present in each retromer cargo, dictate the rate of endosome exit and subsequent delivery to the appropriate downstream destination, but not the destination itself.

Evidence for downstream sorting guiding cargo itinerary after endosome exit

Because β2AR and Wls exit endosomes primarily via same REDs we next investigated trafficking events downstream of cargo exit from endosomes. Wls is considered a retrograde cargo whose delivery to the plasma membrane is assumed to occur after exit from the TGN. However, as a direct endosome-to-plasma membrane route has been clearly demonstrated for the β2AR [31,36], we considered the possibility that Wls may also exhibit some ability to directly recycle. We visualized discrete vesicular insertion events into the plasma membrane by dequenching of superecliptic pHluorin (SpH) fused to the extracellular surface of cargos by rapid TIR-FM imaging as transient bursts of SpH fluorescence produced by

cargo exposure to the neutral extracellular milieu [37–39]. We verified that we could visualize plasma membrane SpH-tagged β2AR and that these indeed represent recycling events by coincident arrival of fluorescent antibody used to label receptors present initially in the plasma membrane (Figure 6A) [31,37]. Remarkably, similar insertion events were observed by imaging SpH-tagged Wls under the same conditions, and we verified that tagged Wls delivered via these insertion events also originated from the previously internalized pool by coincident arrival of surface-applied fluorescent antibody (Figure 6B). Further, the relative fluorescence intensity of SpH-tagged Wls insertion was significantly brighter than that of SpH-tagged β2AR, as determined by measuring the transient fluorescence intensity increase at the site of insertion relative to ambient plasma membrane surround ($\Delta F/F_0$; Figure 6C). This is consistent with the characteristically higher enrichment of Wls relative to β2AR in RED-derived exit vesicles. Moreover, when surface insertion of SpH-Wls was visualized simultaneously with surface-labeled Flag-β2AR, both cargos were detected in the same vesicular fusion events (Figure 6D). These results support the hypothesis that plasma membrane recycling is not restricted to β2AR and suggest that the recycling route is traversed by a cargo that also undergoes retrograde transport.

Conversely, while β2AR undergoes endosome-to-plasma membrane recycling that bypasses the TGN, as do other various recycling cargos [40,41]. FAM21, a component of the WASH complex that activates Arp2/3-mediated actin polymerization at endosomes, was shown recently to also restrict TGN accumulation of PDZ motif-containing cargos, including β2AR [42]. We verified that FAM21 knockdown (Figure 6E) increased localization of Flag-β2AR in membranes marked by TGN46 (Figure 6F), albeit to a reduced degree when compared to TGN localization of HA-Wls (Figures 6G and 6H). Consistent with this effect of FAM21 occurring downstream of endosome exit [42], FAM21 knockdown did not detectably change the localization of either Flag-β2AR or HA-Wls in endosomes, nor did it detectably change their distinct degrees of enrichment in shared REDs (Figures 6I and 6J).

Moreover HA-WlsΔ35, despite lacking either retromer sorting determinant and being unable to detectably transit from endosomes to TGN (Figure 4H), was still present in the TGN when its steady state localization was assessed (Figure 6K and 6L). The source of this TGN-localized HA-WlsΔ35 is presumably the biosynthetic pathway, and thus likely represents a mechanism of accumulation that is independent of retromer. Together, these results indicate retromer-dependent itineraries can be separated downstream of endosome exit.

A discrete effect of retromer sorting determinants on G protein activation from endosomes

Because our data indicate that cargo enrichment in REDs does not dictate downstream itinerary, we wondered if these differences might have some other effect. We were particularly intrigued by the relatively weak ability of the β2AR's PDZ motif-based retromer sorting determinant to drive cargo enrichment in REDs when compared to Wls' Φ-X-[L/M] -based determinant. Because it is now evident that β2AR can initiate signaling via its cognate heterotrimeric G protein, Gs, from endosomes as well as the plasma membrane [28,43], we asked if this weak degree of β2AR enrichment in REDs might somehow be relevant to β2AR's function of signal activation at endosomes.

To do so, we applied previously validated biosensor technology [28] to directly examine the effects of manipulating receptor enrichment in REDs on the initial steps of β2AR-Gs signal activation, focusing on Flag-β2ARΔPDZ that exhibits decreased RED enrichment and Flag-β2ARΔ42-Wls35 that exhibits increased RED enrichment when compared to wild type Flag-β2AR. We first verified that these engineered receptors mediate G protein-dependent signal activation by determining that each drives ligand-dependent stimulation of cyclic AMP accumulation (Figures S6A–6C). We then specifically probed receptor activation at endosomes using a nanobody-derived biosensor (Nb80-GFP) that specifically recognizes conformationally activated receptors in living cells [28,44]. We verified that Nb80-GFP localizes diffusely in the cytoplasm in cells not exposed to agonist and is strongly recruited to Flag-β2AR-containing endosomes after application of isoproterenol [28]. The same phenomenon was observed for both Flag-β2ARΔPDZ and Flag-β2ARΔ42-Wls35 (Figures 7A–7C). When the degree of biosensor recruitment was quantified across images and experiments, by determining a ratio of biosensor intensity to receptor intensity at endosomes, all of the β2AR-derived constructs appeared indistinguishable in their ability to be conformationally activated in endosomes (Figure 7D).

We next probed endosomal activation of Gs, the immediate downstream signal transducer in the β2AR signaling cascade that is activated by direct interaction with β2AR, using a different nanobody-derived biosensor (Nb37-GFP) [28,45]. We verified that Nb37-GFP localizes diffusely in the cytoplasm in the absence of agonist and is recruited to endosomes containing Flag-β2AR following application of isoproterenol (Figure 7F). Interestingly, Nb37-GFP was recruited to endosomes more strongly by Flag-β2ARΔPDZ than the parental Flag-β2AR (Figure 7F). Conversely Flag-β2ARΔ42-Wls35 failed to mediate detectable endosomal recruitment of the Gs activation biosensor in response to isoproterenol (Figure 7G). This was specific because mutating only the Φ-X-[L/M] motifs in this construct, and thus reducing RED enrichment (Flag-β2ARΔ42-Wls35(LQL+YKL>AAA)), enhanced Nb37-GFP recruitment to endosomes (Figures S6D and S6E). We verified these results across multiple images and experiments by again determining a ratio of biosensor to receptor intensity at endosomes (Figure 7H). Together, these data indicate that sequence-directed differences in the degree of β2AR enrichment in REDs, while having no detectable impact on the ability of receptors to undergo conformational activation in endosomes, strongly affects the ability of receptors to subsequently activate their immediate downstream signal transducer, Gs, from the endosome membrane.

DISCUSSION

This study addresses a fundamental question regarding the expanded functions of retromer observed in higher eukaryotes. Our results demonstrate that co-expressed β2AR and Wls, comprising physiologically relevant recycling and retrograde cargos, localize to the same retromer-associated endosomes and can exit via the same transport intermediates generated therefrom. We also show that distinct retromer sorting determinants present in each cargo, which engage retromer through distinct mechanisms, are functionally interchangeable in their capacity to support both itineraries. We then identify a discrete type of kinetic sorting by retromer that controls the rate, but not destination, of retromer-mediated cargo exit and

which influences the ability of β2AR to activate its cognate signal-transducing G protein in endosomes.

The ability of β2AR and Wls to achieve cargo-appropriate trafficking itineraries after shared endosome exit via REDs implies that additional sorting must occur downstream of endosome exit. We think it is likely that multiple downstream sorting operations contribute. We propose five main elements, depicted schematically in Figure 7I. First, both cargos can rapidly transit to the plasma membrane after endocytosis and both are present in the same fusing vesicles, indicating direct endosome-to-plasma membrane recycling. We note that the DMT1-II iron transporter, possessing a Φ-X-[L/M] motif, recycles to the plasma membrane [35] and speculate that DMT1-II may be a naturally occurring example of what we presently demonstrate with engineered cargos. Second, we verify that FAM21 depletion enhances TGN accumulation of β2AR, consistent with its function in suppressing PDZ motif-containing cargo delivery to the TGN [42]. Third, mutant analysis indicates that structural determinants located outside of defined retromer sorting motifs determine downstream itinerary. We note that β2AR and Wls differ transmembrane domain length: 23 amino acids for β2AR and for 21 amino acids for Wls. These correspond closely to the average transmembrane domain lengths of plasma membrane and Golgi resident proteins in mammalian cells [46], and differences in transmembrane length of this order have been demonstrated previously to shift steady state cargo localization from plasma membrane to Golgi distributions [47]. Fourth, Wls has a dibasic motif located in its cytoplasmic tail that is distinct from its Φ-X-[L/M] motifs, and which mediates a discrete, retromer-independent process of Golgi-to-ER retrieval [24]. We deliberately disabled this motif in the present study to prevent this retromer-independent step, which plays a major role in distinguishing the downstream itinerary of Wls from β2AR under normal physiological conditions, to focus on the upstream endosome exit step. Fifth, Wls present in the plasma membrane undergoes rapid and constitutive endocytosis, which provides a means by which Wls delivered to the plasma membrane could be retrieved and sorted again. Accordingly, constitutive endocytosis of Wls would enable an error-checking function of the sorting network and allow the physiologically appropriate retrograde itinerary of Wls to be repeatedly refined through iteration.

The discrete sorting determinants in β2AR and Wls differ markedly in the degree to which they promote cargo enrichment in REDs. Our results demonstrate this to a spatial resolution of ~100 nm; future studies using higher-resolution methods could further solidify this point. This difference mediates a type of kinetic sorting affecting the rate of cargo delivery via both recycling and retrograde routes, but does not dictate downstream cargo itinerary.

Our results also reveal an inverse correlation between B2AR enrichment in REDs and local G protein activation from endosomes. They do not, however, establish whether RED enrichment affects overall cellular signaling. The total cAMP response mediated by all of the B2AR constructs tested was partially inhibited by acute endocytic blockade imposed by Dyngo-4a, but we were unable to detect a statistically significant difference in this metric between constructs with distinct RED enrichments (Figure S6E). Receptor enrichment in REDs is expected to both reduce G protein activation from endosomes and increase it from the plasma membrane (through recycling and resensitization), creating opposing effects that

are both inhibited by Dyngo-4a. Therefore, determining whether or how differential RED enrichment impacts downstream signaling remains an important direction for future study.

In sum, the present results establish that divergent recycling and retrograde trafficking itineraries can be achieved by shared cargo exit from endosomes, using a shared and likely biochemically heterogeneous retromer coat structure, and reveal a previously unrecognized type of kinetic sorting mediated by retromer that has both trafficking and signaling consequences (Figure 7J). In addition to providing insight to functional diversity of retromer in higher eukaryotes, these findings have implications for understanding diseases caused by mutations or altered expression of retromer subunits [5] that have been interpreted mainly according to effects on retrograde membrane transport.

EXPERIMENTAL PROCEDURES

Materials (DNA constructs, siRNAs, and antibodies), SIM imaging, image analysis, immunobloting, and cAMP assays are described in Supplemental Experimental Procedures.

Cell culture and transfection

HEK-293 and HeLa cells (ATCC) were grown in DMEM (Gibco) supplemented with 10% fetal bovine serum (UCSF Cell Culture Facility). Transfection of DNA constructs and siRNAs was performed using Lipofectamine 2000 and RNAi-max (Invitrogen), respectively, according to the manufacturer's instructions. For DNA expression, cells were transfected 48 hours before experiments and for siRNA knockdown, cells were transfected 72 hours before experiments.

Fixed Cell Microscopy

Cells were transfected with the indicated siRNAs and/or DNA construct(s), re-plated onto glass coverslips coated with poly-L-lysine 24 hours post-transfection, and fixed for imaging 24 hours after replating. For surface chase assays, cells were: (1) placed on ice and rinsed with ice-cold phosphate-buffered saline (PBS), (2) labeled by the addition of antibodies in ice-cold PBS for 30 minutes, (3) rinsed with room temperature PBS, and (4) allowed to traffic for specified time point by the addition of 37°C media with or without a saturating concentration of β2AR agonist (10 μM isoproterenol, Sigma). Cells were then rinsed with PBS and fixed by incubation in 3.7% formaldehyde (Fisher Scientific) diluted in modified BRB80 buffer (80 mM PIPES, 1 mM $MgCl_2$, 1 mM $CaCl_2$, pH 6.8) for 15 minutes and then blocked in blocking buffer (3% Bovine Serum Albumin (Sigma) in PBS with or without permeabilization by 0.1% triton X-100 (Sigma)) for 30 minutes. Primary labeling was performed by the addition of antibodies diluted 1:1000 in blocking buffer for one hour and secondary labeling was performed by the addition of antibodies diluted at 1:500 in blocking buffer for 20 minutes. DAPI counterstaining was performed by exposing cells to 300 nM DAPI-dihydrochloride (Sigma) for one minute. Specimens were mounted using ProLong Gold antifade reagent (Life Technologies).

Live cell microscopy

Cells were transfected as indicated, re-plated onto glass bottom dishes (MatTek) coated with poly-L-lysine (Sigma) 24 hours post-transfection, and imaged 24 hours post re-plating. Surface Flag and HA epitopes were labeled on ice as described above, but with Alexa Fluor-conjugated antibodies. Cells were imaged in DMEM without phenol red (UCSF Cell Culture Facility) supplemented with 30 mM HEPES at 37°C.

Image acquisition

Spinning disc confocal images were acquired on a Nikon TE-2000 with confocal scanner unit (Yokogawa) using a 100X NA1.45 objective using an electron multiplying CCD camera (Andor) controlled by Micro-Manager software (https://www.micro-manager.org). Epifluorescence images were acquired on a Nikon inverted microscope with a 60X NA1.4 objective illuminated by a mercury arc lamp through standard dichroic filter sets (Chroma) and collected using a cooled CCD camera (Princeton Instruments). TIR-FM images were collected on a Nikon Ti-E inverted microscope equipped for through-the-objective TIR-FM with a Apo TIRF 100X, NA1.49 objective (Nikon) with solid-state lasers of 405, 488, 561 and 647 nm (Keysight Technologies) using an EMCCD camera (Andor) controlled by NIS-Elements 4.1 software to acquire image sequences every 50 ms for 5 min. Exposure times and illumination were adjusted to remain in the dynamic range of each camera.

Flow Cytometry and Recycling Assays

Cells were transfected as described, re-plated into 12-well dishes 24 hours post-transfection, and analyzed by flow cytometry 24 hours post re-plating. Surface expression was measured by the addition of antibody diluted in PBS at 4°C for 25 minutes. Flow-cytometry-based recycling assays were performed as described previously [10]. Fluorescence intensity profiles of cell populations (>2,500 cells per sample) were measured using a FACS-Calibur instrument (BD Biosciences). In each experiment, duplicate treatments were analyzed for each condition.

Statistical analysis

Results are displayed as mean of results from each experiment or data set, as indicated in figure legends. The statistical significance between conditions for experiments with two conditions was calculated using paired, two tailed t-tests. For experiments with ≥3 conditions, statistical significance was calculated using either Tukey or Dunnett's multiple comparison test, depending on experimental setup, following ordinary one-way ANOVA. For time course experiments, statistical significance was calculated using Dunnett's multiple comparison test following two-way ANOVA. All statistical calculations were performed using Prism6.0 software (GraphPad Software, Inc). The threshold for significance was $p<0.05$ and the coding for significance is reported is: (ns) $p>0.05$, (*) $p\leq0.05$, (**) $p\leq0.01$, (***)$p\leq0.001$, (****) $p\leq0.00001$.

Supplementary Material

Refer to Web version on PubMed Central for supplementary material.

Acknowledgments

We thank Robert Levenson for providing the Wls antibody. We thank Aaron Marley and Daniel Elnatan for cloning advice and Braden Lobingier for devising the RED enrichment index metric. We thank Pat O'Farrell, Robert Edwards, David Mavor, and members of the MvZ lab for useful discussion. We thank DeLaine Larsen for assistance with imaging experiments. TIR-FM and SIM imaging experiments were carried out at the UCSF Nikon Imaging Center directed by Kurt Thorn. The work was supported by the US National Institutes of Health (DA036290 to KV, HL122508 to RI, and DA012864 and DA010711 to MvZ).

REFERENCES

1. Seaman MN, McCaffery JM, Emr SD. A membrane coat complex essential for endosome-to-Golgi retrograde transport in yeast. J. Cell Biol. 1998; 142:665–681. [PubMed: 9700157]
2. Seaman MN, Marcusson EG, Cereghino JL, Emr SD. Endosome to Golgi retrieval of the vacuolar protein sorting receptor, Vps10p, requires the function of the VPS29, VPS30, and VPS35 gene products. J. Cell Biol. 1997; 137:79–92. [PubMed: 9105038]
3. Nothwehr SF, S-A H, Bruinsma P. Sorting of Yeast Membrane Proteins into an Endosome-to-Golgi Pathway Involves Direct Interaction of Their Cytosolic Domains with Vps35p. J. Cell Biol. 2000; 151:297–310. [PubMed: 11038177]
4. Horazdovsky BF, Davies BA, Seaman MN, McLaughlin SA, Yoon S, Emr SD. A sorting nexin-1 homologue, Vps5p, forms a complex with Vps17p and is required for recycling the vacuolar protein-sorting receptor. Mol. Biol. Cell. 1997; 8:1529–1541. [PubMed: 9285823]
5. Trousdale C, Christopher T, Kyoungtae K. Retromer: Structure, function, and roles in mammalian disease. Eur. J. Cell Biol. 2015; 94:513–521. [PubMed: 26220253]
6. Haft CR, M dl, Bafford R, Lesniak MA, Barr VA, Taylor SI. Human Orthologs of Yeast Vacuolar Protein Sorting Proteins Vps26; 29, and 35: Assembly into Multimeric Complexes. Mol. Biol. Cell. 2000; 11:4105–4116. [PubMed: 11102511]
7. Haft CR, de la Luz Sierra M, Barr VA, Haft DH, Taylor SI. Identification of a family of sorting nexin molecules and characterization of their association with receptors. Mol. Cell Biol. 1998; 18:7278–7287. [PubMed: 9819414]
8. Gallon M, Cullen PJ. Retromer and sorting nexins in endosomal sorting. Biochem. Soc. Trans. 2015; 43:33–47. [PubMed: 25619244]
9. Chen D, Xiao H, Zhang K, Wang B, Gao Z, Jian Y, Qi X, Sun J, Miao L, Yang C. Retromer is required for apoptotic cell clearance by phagocytic receptor recycling. Science. 2010; 327:1261–1264. [PubMed: 20133524]
10. Temkin P, Paul T, Ben L, Stefanie J, Peter C, Krogan NJ, von Zastrow M. SNX27 mediates retromer tubule entry and endosome-to-plasma membrane trafficking of signalling receptors. Nat. Cell Biol. 2011; 13:717–723.
11. Rojas R, Kametaka S, Haft CR, Bonifacino JS. Interchangeable but essential functions of SNX1 and SNX2 in the association of retromer with endosomes and the trafficking of mannose 6-phosphate receptors. Mol. Cell Biol. 2007; 27:1112–1124. [PubMed: 17101778]
12. Wassmer T, Attar N, Bujny MV, Oakley J, Traer CJ, Cullen PJ. A loss-of-function screen reveals SNX5 and SNX6 as potential components of the mammalian retromer. J Cell Sci. 2007; 120:45–54. [PubMed: 17148574]
13. Swarbrick JD, Shaw DJ, Chhabra S, Ghai R, Valkov E, Norwood SJ, Seaman MNJ, Collins BM. VPS29 is not an active metallo-phosphatase but is a rigid scaffold required for retromer interaction with accessory proteins. PLoS One. 2011; 6:e20420. [PubMed: 21629666]
14. Harterink M, Port F, Lorenowicz MJ, McGough IJ, Silhankova M, Betist MC, van Weering JRT, van Heesbeen RGHP, Middelkoop TC, Basler K, et al. A SNX3-dependent retromer pathway mediates retrograde transport of the Wnt sorting receptor Wntless and is required for Wnt secretion. Nat. Cell Biol. 2011; 13:914–923. [PubMed: 21725319]
15. Zhang P, Peng Z, Yihui W, Belenkaya TY, Xinhua L. SNX3 controls Wingless/Wnt secretion through regulating retromer-dependent recycling of Wntless. Cell Res. 2011; 21:1677–1690. [PubMed: 22041890]

16. Gallon M, Clairfeuille T, Steinberg F, Mas C, Ghai R, Sessions RB, Teasdale RD, Collins BM, Cullen PJ. A unique PDZ domain and arrestin-like fold interaction reveals mechanistic details of endocytic recycling by SNX27-retromer. Proc. Natl. Acad. Sci. U.S.A. 2014; 111:E3604–E3613. [PubMed: 25136126]
17. Lauffer BEL, Melero C, Temkin P, Lei C, Hong W, Kortemme T, von Zastrow M. SNX27 mediates PDZ-directed sorting from endosomes to the plasma membrane. J. Cell Biol. 2010; 190:565–574. [PubMed: 20733053]
18. Franch-Marro X, Wendler F, Guidato S, Griffith J, Baena-Lopez A, Itasaki N, Maurice MM, Vincent J-P. Wingless secretion requires endosome-to-Golgi retrieval of Wntless/Evi/Sprinter by the retromer complex. Nat. Cell Biol. 2008; 10:170–177. [PubMed: 18193037]
19. Port F, Kuster M, Herr P, Furger E, Bänziger C, Hausmann G, Basler K. Wingless secretion promotes and requires retromer-dependent cycling of Wntless. Nat. Cell Biol. 2008; 10:178–185. [PubMed: 18193032]
20. Belenkaya TY, Wu Y, Tang X, Zhou B, Cheng L, Sharma YV, Yan D, Selva EM, Lin X. The retromer complex influences Wnt secretion by recycling wntless from endosomes to the trans-Golgi network. Dev. Cell. 2008; 14:120–131. [PubMed: 18160348]
21. Pan C-L, Baum PD, Gu M, Jorgensen EM, Clark SG, Garriga G. C. elegans AP-2 and retromer control Wnt signaling by regulating mig-14/Wntless. Dev. Cell. 2008; 14:132–139. [PubMed: 18160346]
22. Yang P-T, Lorenowicz MJ, Silhankova M, Coudreuse DYM, Betist MC, Korswagen HC. Wnt signaling requires retromer-dependent recycling of MIG-14/Wntless in Wnt-producing cells. Dev. Cell. 2008; 14:140–147. [PubMed: 18160347]
23. Violin JD, DiPilato LM, Yildirim N, Elston TC, Zhang J, Lefkowitz RJ. beta2-adrenergic receptor signaling and desensitization elucidated by quantitative modeling of real time cAMP dynamics. J. Biol. Chem. 2008; 283:2949–2961. [PubMed: 18045878]
24. Yu J, Chia J, Canning CA, Jones CM, Bard FA, Virshup DM. WLS retrograde transport to the endoplasmic reticulum during Wnt secretion. Dev. Cell. 2014; 29:277–291. [PubMed: 24768165]
25. Wls. The Human Protein Atlas. [accessed June 1, 2016] n.d. http://www.proteinatlas.org/ENSG00000116729-WLS/tissue.
26. ADRB2. The Human Protein Atlas. [accessed June 1, 2016] n.d. http://www.proteinatlas.org/ENSG00000169252-ADRB2/tissue.
27. von Zastrow M, Kobilka BK. Ligand-regulated internalization and recycling of human beta 2-adrenergic receptors between the plasma membrane and endosomes containing transferrin receptors. J. Biol. Chem. 1992; 267:3530–3538. [PubMed: 1371121]
28. Irannejad R, Tomshine JC, Tomshine JR, Chevalier M, Mahoney JP, Steyaert J, Rasmussen SGF, Sunahara RK, El-Samad H, Huang B, et al. Conformational biosensors reveal GPCR signalling from endosomes. Nature. 2013; 495:534–538. [PubMed: 23515162]
29. Gasnereau I, Herr P, Chia PZC, Basler K, Gleeson PA. Identification of an endocytosis motif in an intracellular loop of Wntless protein, essential for its recycling and the control of Wnt protein signaling. J. Biol. Chem. 2011; 286:43324–43333. [PubMed: 22027831]
30. Cao TT, Brelot A, von Zastrow M. The composition of the beta-2 adrenergic receptor oligomer affects its membrane trafficking after ligand-induced endocytosis. Mol. Pharmacol. 2005; 67:288–297. [PubMed: 15492118]
31. Puthenveedu MA, Lauffer B, Temkin P, Vistein R, Carlton P, Thorn K, Taunton J, Weiner OD, Parton RG, von Zastrow M. Sequence-dependent sorting of recycling proteins by actin-stabilized endosomal microdomains. Cell. 2010; 143:761–773. [PubMed: 21111236]
32. Gustafsson MGL, Lin S, Carlton PM, Rachel Wang CJ, Golubovskaya IN, Zacheus Cande W, Agard DA, Sedat JW. Three-Dimensional Resolution Doubling in Wide-Field Fluorescence Microscopy by Structured Illumination. Biophys. J. 2008; 94:4957–4970. [PubMed: 18326650]
33. Cao TT, Deacon HW, Reczek D, Bretscher A, von Zastrow M. A kinase-regulated PDZ-domain interaction controls endocytic sorting of the beta2-adrenergic receptor. Nature. 1999; 401:286–290. [PubMed: 10499588]
34. Seaman MNJ. Identification of a novel conserved sorting motif required for retromer-mediated endosome-to-TGN retrieval. J. Cell Sci. 2007; 120:2378–2389. [PubMed: 17606993]

35. Tabuchi M, Yanatori I, Kawai Y, Kishi F. Retromer-mediated direct sorting is required for proper endosomal recycling of the mammalian iron transporter DMT1. J. Cell Sci. 2010; 123:756–766. [PubMed: 20164305]
36. Choy RW-Y, Minjong P, Paul T, Herring BE, Aaron M, Nicoll RA, von Zastrow M. Retromer Mediates a Discrete Route of Local Membrane Delivery to Dendrites. Neuron. 2014; 82:55–62. [PubMed: 24698268]
37. Yudowski GA, Puthenveedu MA, von Zastrow M. Distinct modes of regulated receptor insertion to the somatodendritic plasma membrane. Nat. Neurosci. 2006; 9:622–627. [PubMed: 16604070]
38. Miesenböck G, De Angelis DA, Rothman JE. Visualizing secretion and synaptic transmission with pH-sensitive green fluorescent proteins. Nature. 1998; 394:192–195. [PubMed: 9671304]
39. Sankaranarayanan S, De Angelis D, Rothman JE, Ryan TA. The use of pHluorins for optical measurements of presynaptic activity. Biophys. J. 2000; 79:2199–2208. [PubMed: 11023924]
40. Geuze HJ, Slot JW, Strous GJ, Peppard J, von Figura K, Hasilik A, Schwartz AL. Intracellular receptor sorting during endocytosis: comparative immunoelectron microscopy of multiple receptors in rat liver. Cell. 1984; 37:195–204. [PubMed: 6327050]
41. Snider MD, Rogers OC. Intracellular movement of cell surface receptors after endocytosis: resialylation of asialo-transferrin receptor in human erythroleukemia cells. J. Cell Biol. 1985; 100:826–834. [PubMed: 2982885]
42. Lee S, Chang J, Blackstone C. FAM21 directs SNX27-retromer cargoes to the plasma membrane by preventing transport to the Golgi apparatus. Nat. Commun. 2016; 7:10939. [PubMed: 26956659]
43. Tsvetanova NG, von Zastrow M. Spatial encoding of cyclic AMP signaling specificity by GPCR endocytosis. Nat. Chem. Biol. 2014; 10:1061–1065. [PubMed: 25362359]
44. Rasmussen SGF, Choi H-J, Fung JJ, Pardon E, Casarosa P, Chae PS, Devree BT, Rosenbaum DM, Thian FS, Kobilka TS, et al. Structure of a nanobody-stabilized active state of the β(2) adrenoceptor. Nature. 2011; 469:175–180. [PubMed: 21228869]
45. Rasmussen SGF, DeVree BT, Yaozhong Z, Kruse AC, Chung KY, Kobilka TS, Thian FS, Chae PS, Els P, Diane C, et al. Crystal structure of the β2 adrenergic receptor–Gs protein complex. Nature. 2011; 477:549–555. [PubMed: 21772288]
46. Sharpe HJ, Stevens TJ, Munro S. A comprehensive comparison of transmembrane domains reveals organelle-specific properties. Cell. 2010; 142:158–169. [PubMed: 20603021]
47. Masibay AS, Balaji PV, Boeggeman EE, Qasba PK. Mutational analysis of the Golgi retention signal of bovine beta-1,4-galactosyltransferase. J. Biol. Chem. 1993; 268:9908–9916. [PubMed: 8387508]

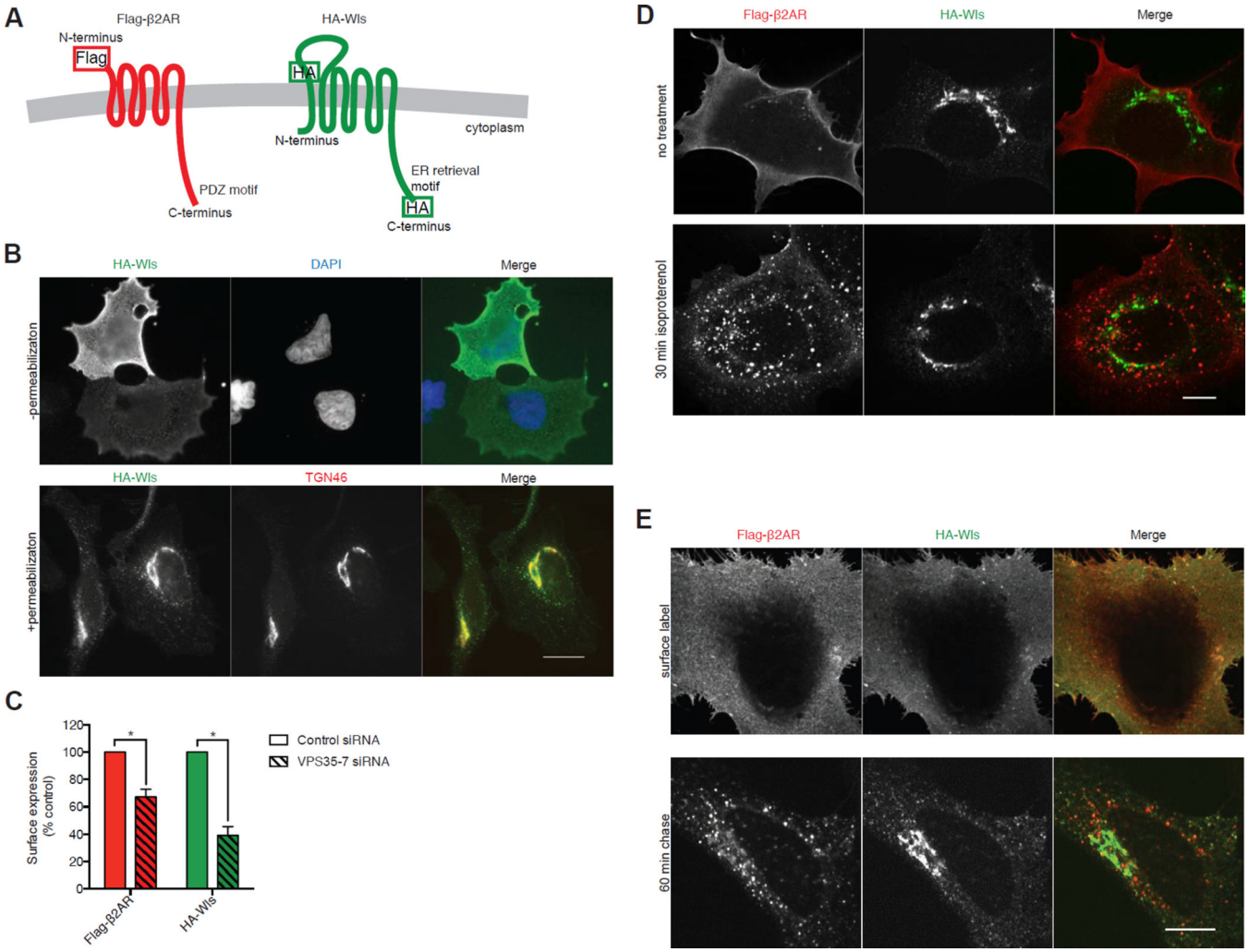

Figure 1. Direct comparison of retromer-dependent recycling and retrograde transport cargos in the same cells

(**A**) Schematic representation of Flag-β2AR (left) and HA-Wls (right) showing topology and epitope tagging. (**B**) Representative widefield images of HeLa cells expressing HA-Wls, stained without (top) or with (bottom) permeabilization. (**C**) Average Flag-β2AR and HA-Wls surface fluorescence upon control or VPS35 knockdown, as percent of control surface expression measured by fluorescence flow cytometry (n=3 independent experiments). Error bars represent s.e.m. (**D**) Representative confocal images of permeabilized HEK-293 cells with no treatment (top) or with 30 minutes of saturating (10 μM) isoproterenol treatment (bottom), showing the localization of Flag-β2AR and HA-Wls. (**E**) Representative confocal images of HeLa cells expressing Flag-β2AR and HA-Wls, surface labeled with anti- Flag and - HA antibodies, and fixed after 0-minute (top) or 60-minute (bottom) chase incubation. Scale Bars, 10 μm. See also Figures S1 and S2.

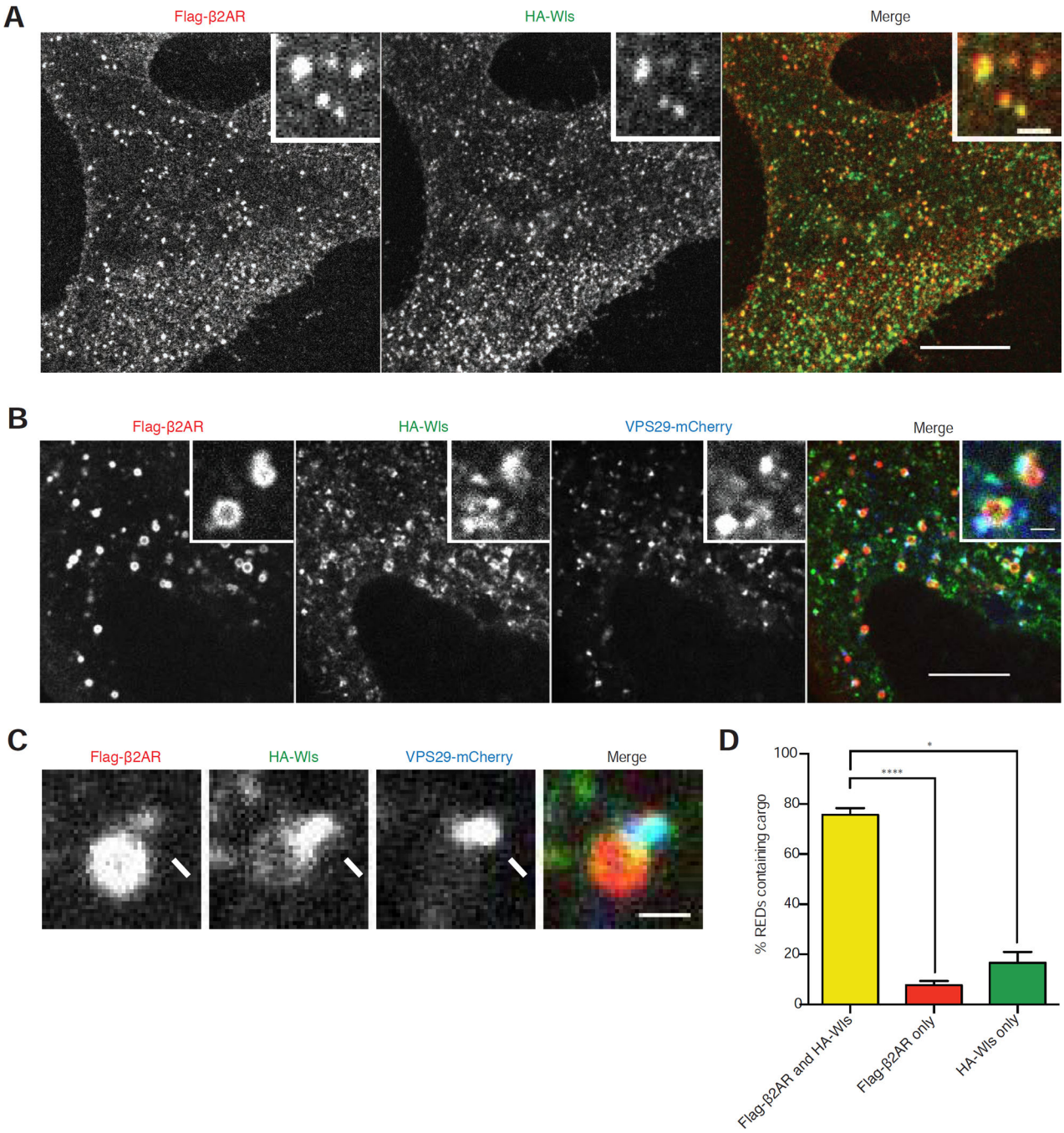

Figure 2. β2AR and Wls traffic through the same endosomes and retromer endosome domains

(**A**) Representative confocal image of a HeLa cell expressing Flag-β2AR and HA-Wls surface labeled with anti- Flag and HA antibodies and fixed after 15-minute chase incubation. Inset shows a representative region at higher magnification. (**B**) Representative confocal image of live a HEK-293 cell expressing Flag-β2AR, HA-Wls, and VPS29-mCherry surface labeled with anti- Flag and HA antibodies after chase incubation. Inset shows a representative region at higher magnification. (**C**) Enlarged view of an endosome in a HEK-293 cell with a RED (arrows) containing both Flag-β2AR and HA-Wls. (**D**)

Quantification of cargos in REDs after 7–51 minute chase incubations (n=3 independent experiments). Error bars correspond to s.e.m. Large image scale bars, 10 μm; inset scale bars, 1 μm. See also Movie S1.

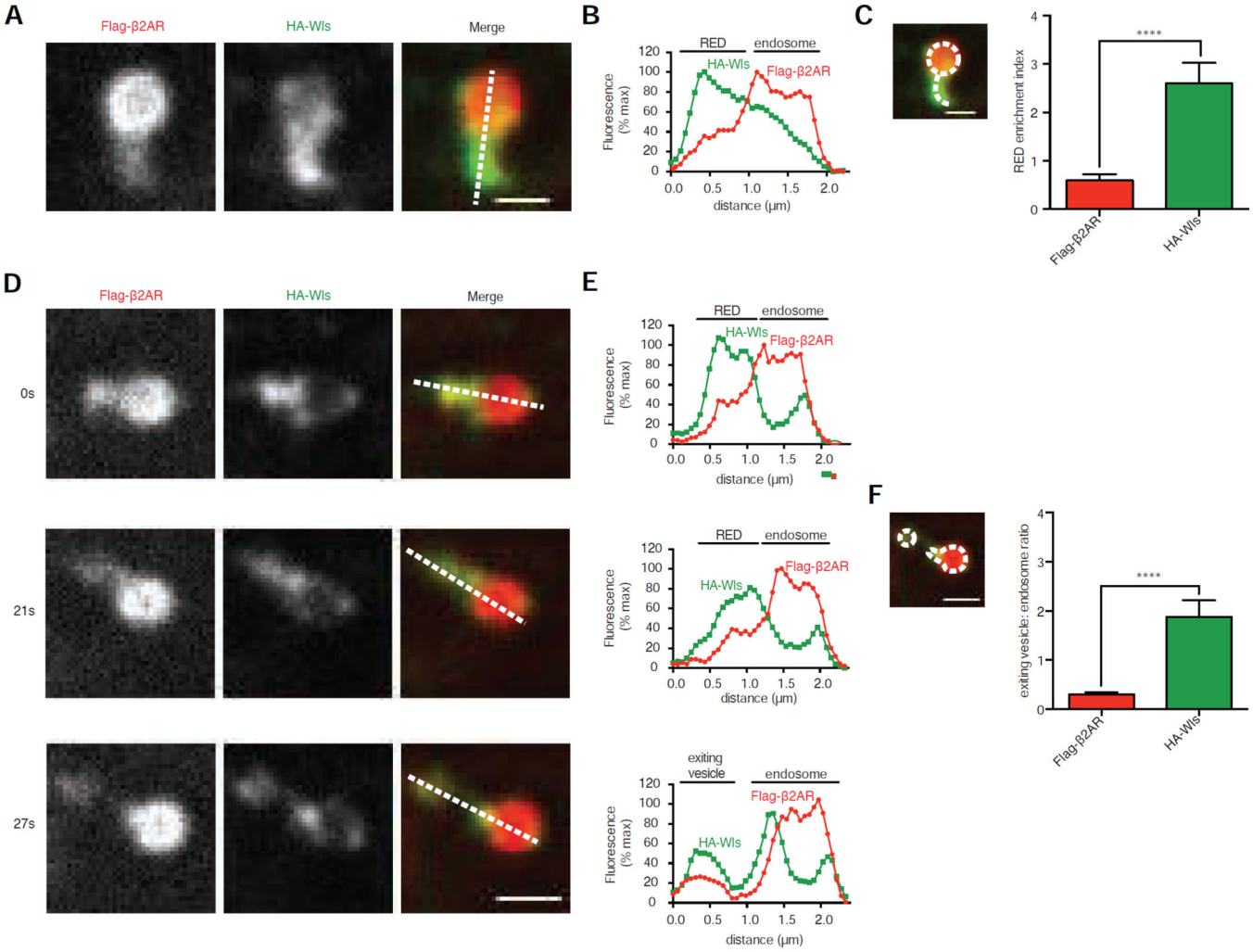

Figure 3. β2AR and Wls have distinct abilities to enrich in and exit from REDs

(**A**) Representative confocal image of an endosome in a HEK-293 cell surface labeled for Flag-β2AR and HA-Wls. Dotted line in merge panel shows line used for fluorescence intensity profile in B. (**B**) Fluorescence intensity profile, normalized to maximum, of line shown in panel A. (**C**) Average RED enrichment indices of Flag-β2AR and HA-Wls, defined as the ratio of the mean, background-subtracted fluorescence per pixel in the RED divided by the mean, background-subtracted fluorescence per pixel in the adjacent endosome (n=30 REDs pooled from 3 independent experiments). Inset image shows an example of the regions of interest used to quantify the endosome (dotted circle) and RED (dotted curved line). (**D**) Representative time-lapse series of a RED scission event, with relative time in seconds denoted to left of each image. Dotted lines in merge image panels show lines used for fluorescence intensity profiles in E. (**E**) Fluorescence intensity profiles, normalized to series maximum, of lines shown in panel D. (**F**) Average exiting vesicle to endosome ratios of Flag-β2AR and HA-Wls, defined as the ratio of the mean, background-subtracted exiting vesicle fluorescence per pixel divided by the mean, background-subtracted endosome fluorescence per pixel (n=24 events pooled from 3 independent experiments). Inset image show an example of the regions of interest used for the endosome

(large dotted shape) and RED (small dotted shape). Error bars correspond to s.e.m. Scale bars, 1 μm. See also Figure S3 and Movie S2.

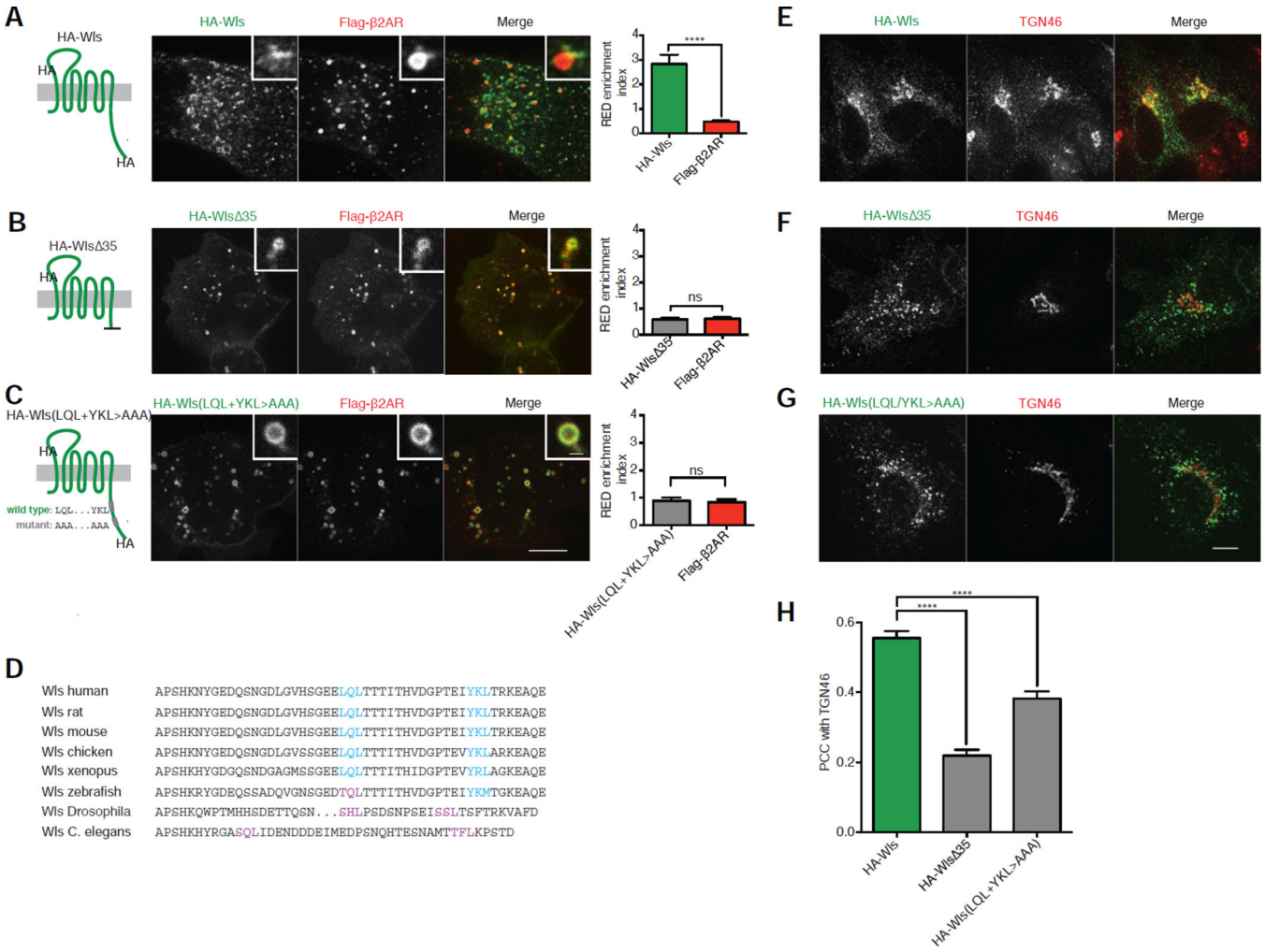

Figure 4. Identification of Φ-X-[L/M] motifs in Wls' cytoplasmic tail required for strong RED enrichment and retrograde transport

(**A–C**) Left, schematic representations of HA-Wls wild type, HA-WlsΔ35, and HA-Wls(LQL+YKL>AAA) showing the corresponding mutations, topology, and epitope tagging. Center, representative confocal images of live HEK-293 cells surface labeled for HA-Wls wild type, HA-WlsΔ35, or HA-Wls(LQL+YKL>AAA) and Flag-β2AR after chase incubations. Inset images show representative endosomes with REDs at higher magnification. Right, average RED enrichment indices of HA-Wls wild type, HA-WlsΔ35, and HA-Wls(LQL+YKL>AAA) compared to Flag-β2AR in the same REDs (*n*=30 REDs pooled from 3 independent experiments). (**D**) Amino acid sequence alignment of the cytoplasmic tails of Wls from different species with Φ-X-[L/M] motifs highlighted in cyan and putative [S/T]-X-[L/M] motifs highlighted in purple. (**E–G**) Representative confocal images of fixed HeLa cells expressing HA-Wls wild type, HA-WlsΔ35, or HA-Wls(LQL +YKL>AAA) surface labeled with anti-HA antibodies and chased for 60 minutes. (**H**) Accumulation of each cargo in the TGN, quantified by average Pearson's correlation coefficient with TGN46 after a 60-minute chase incubation (*n*=30 cells pooled from 3 independent experiments). Large image scale bars, 10 μm; inset scale bars, 1 μm. Error bars correspond to s.e.m. See also Figure S4.

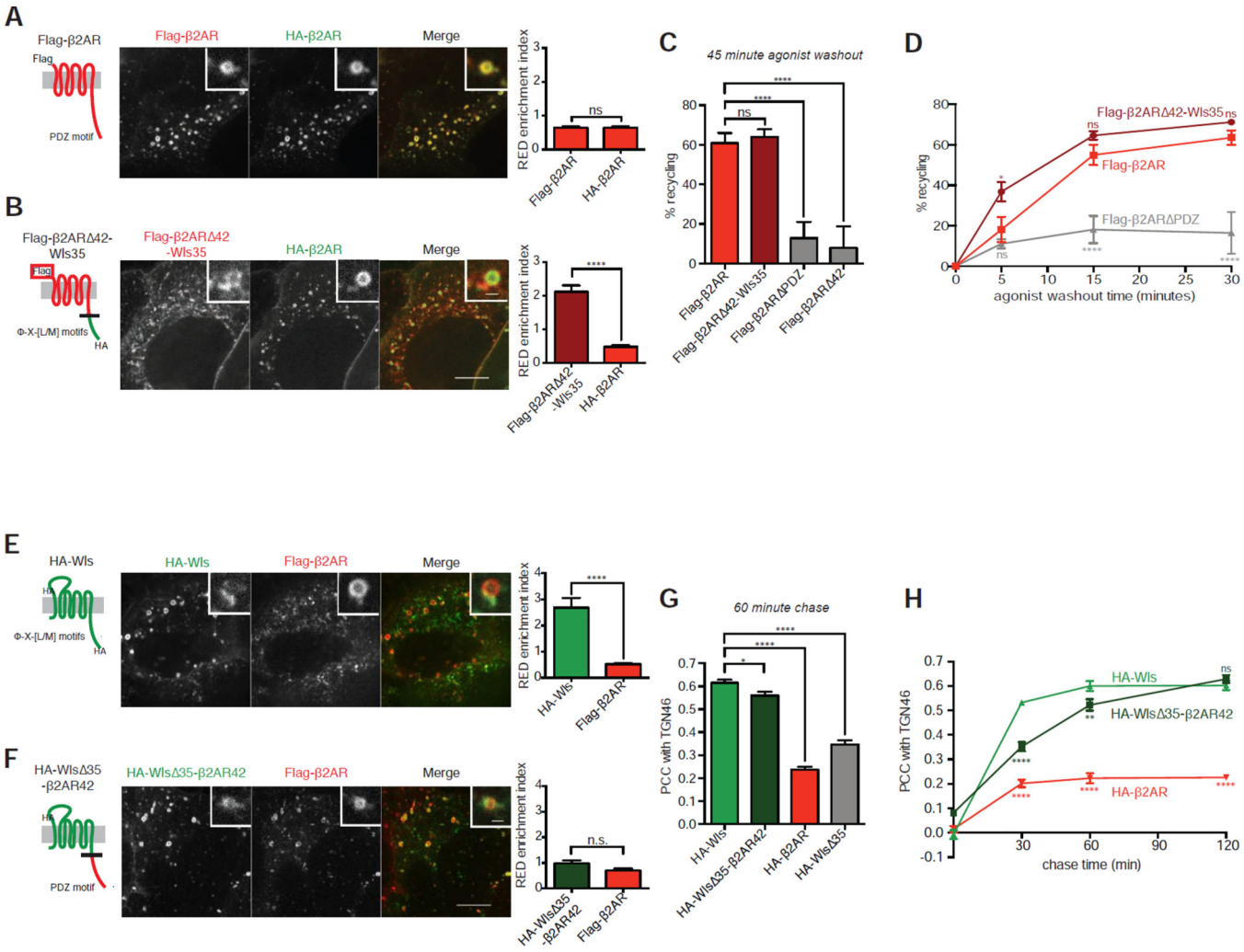

Figure 5. Wls' and β2AR's cytoplasmic tails determine RED enrichment and trafficking kinetics, but not target destination

(**A, B**) Left, schematic representations of Flag-β2AR wild type or Flag-β2ARΔ42-Wls35 showing corresponding mutations, topology, and epitope tagging. Center, representative confocal images of live HEK-293 cells surface labeled for Flag-β2AR wild type or Flag-β2ARΔ42-Wls35 and HA-β2AR after chase incubations. Inset images show representative endosomes with REDs at higher magnification. Right, average RED enrichment indices of Flag-β2AR wild type or Flag-β2ARΔ42-Wls35 compared to HA-β2AR in the same REDs (n=30 REDs pooled from 3 independent experiments). (**C**) Average percent recycled Flag-β2AR wild type or mutant after 45 minutes of agonist washout (n=5). (**D**) Average percent recycled Flag-β2AR wild type or mutant after denoted time points of agonist washout, with statistical significance shown in relation to wild type Flag-β2AR (n=4). (**E, F**) Left, schematic representations of HA-Wls wild type or HA-WlsΔ35-β2AR42 showing corresponding mutations, topology, and epitope tagging. Center, representative confocal images of live HEK-293 cells surface labeled for HA-Wls wild type or HA-WlsΔ35-β2AR42 and Flag-β2AR after chase incubation. Inset images show representative endosomes with REDs at higher magnification. Right, average RED enrichment indices of

HA-Wls wild type or HA-WlsΔ35-β2AR42 compared to Flag-β2AR in the same REDs (*n*=30 REDs pooled from 3 independent experiments). (**G**) Average Pearson's correlation coefficient of each cargo with TGN46 after 60-minute chase incubation, indicating accumulation of each cargo in the TGN (*n*=30 cells pooled from 3 independent experiments). (**H**) Average Pearson's correlation coefficient of each cargo with TGN46 after denoted time points of chase incubation, with statistical significance shown in relation to wild type HA-Wls (*n*=30 cells pooled from 3 independent experiments). Large image scale bars, 10 μm; inset scale bars, 1 μm. Error bars correspond to s.e.m. See also Figure S5.

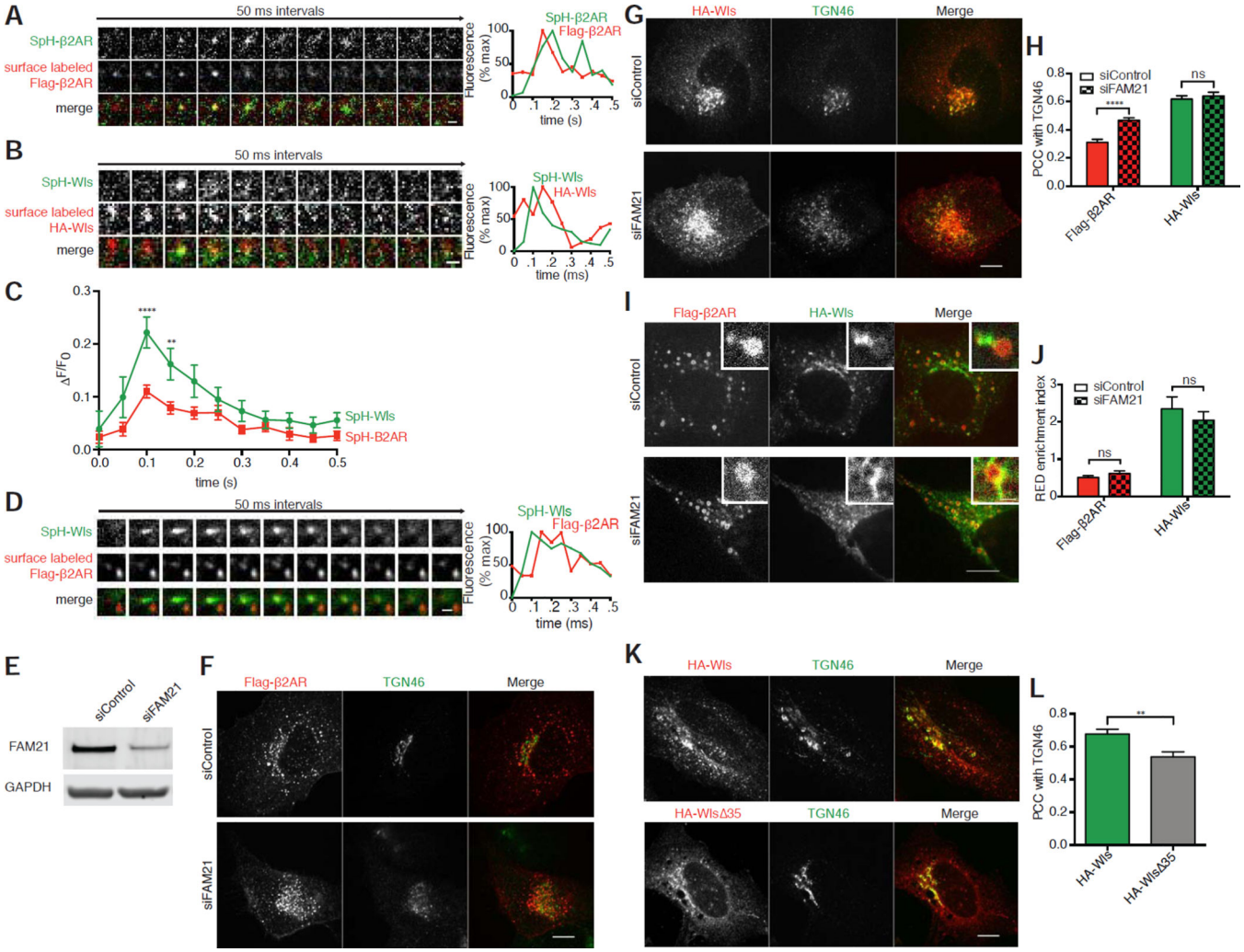

Figure 6. β2AR and Wls are each able to transit both the plasma membrane and the TGN

(**A**) Left, representative TIR-FM image montage showing coincident plasma membrane insertion of Sph-B2AR and surface labeled Flag in a live HEK-293 expressing Flag-SpH-β2AR. Right, fluorescence traces showing that surface labeled Flag appears in the TIRF field prior to SpH insertion and that both signals rapidly diffuse. (**B**) Left, representative TIR-FM image montage showing coincident plasma membrane insertion of Sph-Wls and surface labeled HA in a live HEK-293 expressing HA-SpH-Wls. Right, fluorescence traces showing that surface labeled HA appears in the TIRF field prior to SpH insertion and that both signals rapidly diffuse. (**C**) Average $\Delta F/F_0$ plot of SpH signals of insertion events from cells expressing either SpH-Flag-β2AR or SpH-HA-Wls (n=10 events from two independent experiments). (**D**) Representative TIR-FM image montage showing coincident plasma membrane insertion of Sph and surface labeled Flag (arrows) in a live HEK-293 expressing both HA-SpH-Wls and Flag-β2AR. Right, fluorescence traces showing that surface labeled Flag appears in the TIRF field prior to SpH insertion and that both signals rapidly diffuse. (**E**) Representative immunoblots of cell lysates upon control or FAM21 siRNA knockdown blotted for FAM21 or GAPDH. Average percent knockdown upon treatment with FAM21 siRNA was quantified at 83.0±13.6% of control (mean ± standard deviation, n=3). (**F**)

Representative confocal images of fixed HeLa cells expressing Flag-β2AR, treated with control or FAM21 siRNA, and surface labeled with anti-Flag antibody, chased for 60 minutes. (**G**) Representative confocal images of fixed HeLa cells expressing HA-Wls, treated with control or FAM21 siRNA, and surface labeled with anti-Flag antibody, chased for 60 minutes. (**H**) Accumulation of each cargo in the TGN upon control or FAM21 knockdown, quantified by average Pearson's correlation coefficient with TGN46 after a 60-minute chase incubation (n=30 cells pooled from 3 independent experiments). (**I**) Representative confocal images of live HEK-293 cells treated with either control or FAM21 siRNA surface labeled for HA-Wls and Flag-β2AR after chase incubation. Inset images show representative endosomes with REDs at higher magnification. Inset scale bar,1 μm. (**J**) Average RED enrichment indices of Flag-β2AR and HA-Wls upon control or FAM21 knockdown (n=30 REDs pooled from 3 independent experiments). (**K**) Representative confocal images of permeabilized HeLa cells expressing either HA-Wls or HA-WlsΔ35 showing steady state localization relative to TGN46. (**L**) Average Pearson's correlation coefficient of HA-Wls and HA-WlsΔ35 with TGN46 at steady state (n=20 cells pooled from 2 independent experiments). Large image scale bars; 10 μm. TIR-FM montage scale bars, 1 μm. Error bars correspond to s.e.m.

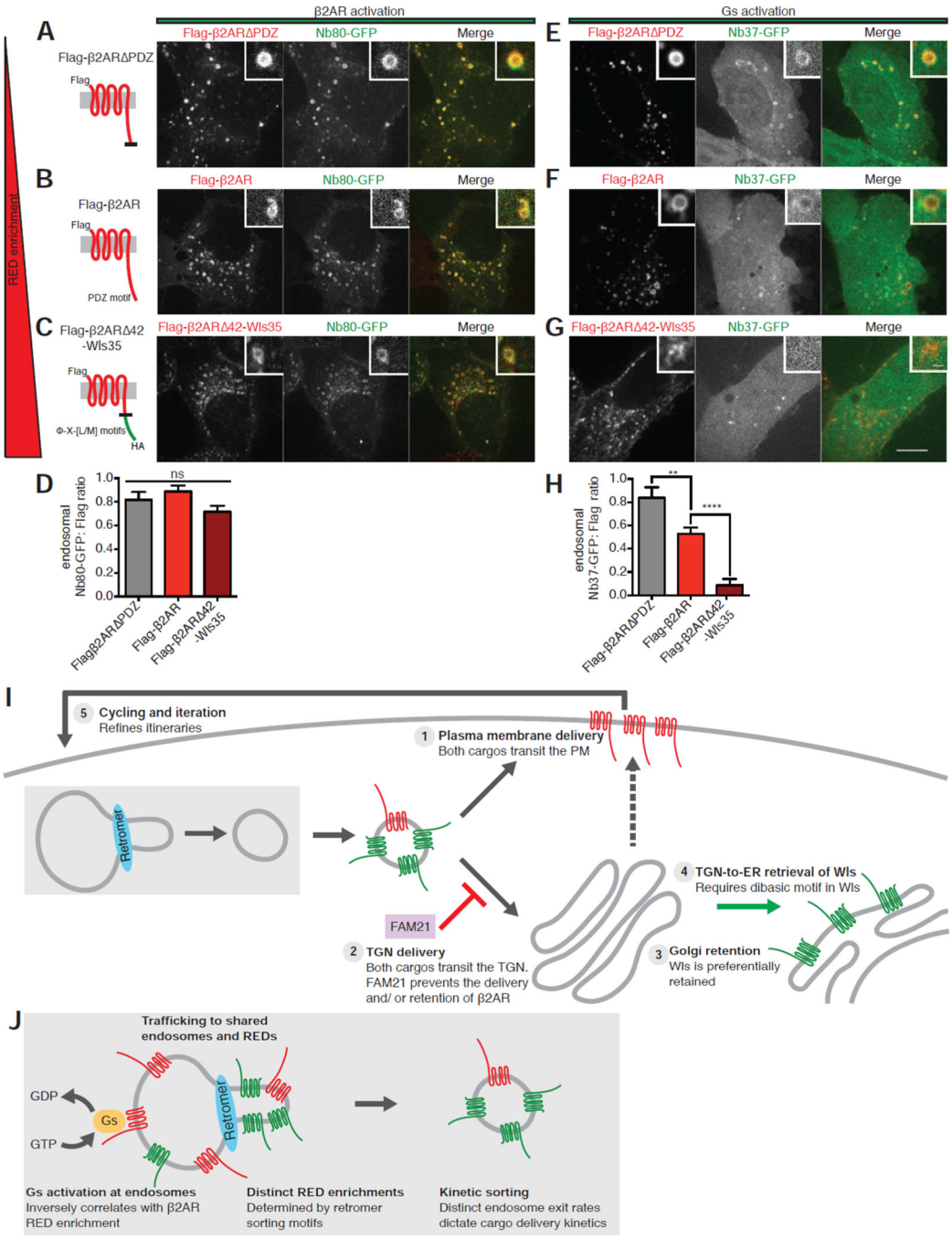

Figure 7. β2AR mutant RED enrichment is inversely correlated with G protein activation at endosomes

(**A–C**) Left, schematic representations of Flag-β2ARΔPDZ, Flag-β2AR wild type, or Flag-β2ARΔ42-Wls35 showing corresponding mutations, topology, and epitope tagging. Note that constructs are ordered by increasing RED enrichment from top to bottom. Right, representative confocal images of live HEK-293 cells expressing Flag-β2ARΔPDZ, Flag-β2AR wild-type, or Flag-β2ARΔ42-Wls35 and Nb80-GFP after Flag surface labeling and subsequent chase incubation. Inset images show representative endosomes at higher

magnification. (**D**) Average Nb80-GFP to Flag fluorescence enrichment ratio in endosomes, (n=30 cells from 3 independent experiments). (**E–G**) Representative confocal images of live HEK-293 cells expressing Flag-β2ARΔPDZ, Flag-β2AR wild type, or Flag-β2ARΔ42-Wls35 and Nb37-GFP after surface Flag labeling and subsequent chase incubation. Inset images show representative endosomes at higher magnification. (**H**) Average Nb37-GFP to Flag fluorescence enrichment ratio in endosomes (n=30 cells from 3 independent experiments). Large image scale bars, 10 μm; inset scale bars, 1 μm. Error bars correspond to s.e.m. (**I**) Schematic model summarizing key findings relating to sorting of β2AR and Wls downstream of shared cargo exit from endosomes. Events depicted as numbered items in model correspond to those discussed in the text. (**J**) Schematic model summarizing key findings relating to retromer's regulation of kinetic sorting and β2AR signal activation at the endosome. See also Figure S6.